Backscatter and Attenuation Imaging from Ultrasonic Scanning in Medicine

Images of backscatter, attenuation, and frequency dependence of attenuation are obtained based on a three-parameter model and computation techniques described in this paper. There are several critical sources of error: backscatter speckle, beamwidth distortion, and cross-coupling artifacts between attenuation and backscatter. An iterative method of imaging and filtering is developed which effectively reduces these errors. Stability of the numerical solution involving the large number of unknowns is obtained by image iteration as opposed to parameter iteration along individual transmitter rays. This method incorporates three basic functional aspects: (1) multiple scans to reduce speckle, beamwidth distortions, and certain cross-coupling artifacts, (2) pre-image filtering to decrease beam distortions and post-image filtering to reduce cross-coupling artifacts, and (3) proper sequencing of image reconstruction and filtering. Backscatter images formed by this image iteration method are significantly superior to standard B-scan images. Further, the image iteration method yields three images of the same scan field. The present investigation is based on simulated echo data from cyst-like and complex targets.

Introduction

Imaging from ultrasound scanning is an important medical method for the detection and diagnosis of a wide range of pathologies. In contrast to x-ray imaging, it has no known harmful effects at diagnostic radiation levels and provides a true cross-sectional image. Current clinical methods are based on echo data (similar to sonar) and generate a qualitative image that reflects the combined effects of backscatter and attenuation.

In the study reported in this paper, an image iteration method was developed which provides quantitative images of backscatter with reduced image artifacts. In addition, images of attenuation and frequency-dependent attenuation are formed from the same scan data. With quantitative, multiparameter imaging, the radiologist has a greater potential for early detection and diagnosis of pathologies.

Echo data yield a large number of values across the scan field. Conceptually, images of backscatter, attenuation, and frequency dependence of attenuation can be obtained based on a three-parameter model. Practically, there are several critical sources of error: backscatter speckle, beamwidth distortion, object shadowing, and cross-coupling artifacts

between attenuation and backscatter. An iterative method of imaging and filtering is developed which effectively reduces these errors.

This method incorporates three basic functional aspects: (1) The number and separation of the echo scans are selected to reduce speckle, beamwidth distortions, and certain cross-coupling artifacts. (2) Pre-image filtering is used to decrease beam distortions; post-image median filtering markedly reduces speckle and cross-coupling artifacts. (3) The optimal sequencing of image reconstruction and filtering is sought.

Backscatter images formed by the image iteration method are significantly superior to those from current imaging methods. Further, the image iteration method yields three images of the same scan field. The present investigation is based on simulated echo data from cyst-like and complex targets. Studies with clinical scans and calibrated tissue phantoms are in progress.

Prior research of Duck, Hill, and Rowe [1, 2] had the same objective as the study reported here. They used an iterative error correction approach which we found to be less

[©] Copyright 1982 by International Business Machines Corporation. Copying in printed form for private use is permitted without payment of royalty provided that (1) each reproduction is done without alteration and (2) the *Journal* reference and IBM copyright notice are included on the first page. The title and abstract, but no other portions, of this paper may be copied or distributed royalty free without further permission by computer-based and other information-service systems. Permission to *republish* any other portion of this paper must be obtained from the Editor.

accurate and less stable than image iteration. Maderlechner [3] describes an accurate tomographic method, but it requires scanning over very large angles and requires extensive computer computations. Kuc [4] demonstrated a method of estimating attenuation in various segments of the liver; an overall attenuation image was not generated. Using synthetic focus imaging with a transducer array, Johnson et al. [5] have investigated methods of imaging absorption and reflection.

Imaging from echo data

Forming images of attenuation and backscatter from echo data is more complex than transmission tomography because two independent images must be estimated, attenuation and backscatter. On the other hand, each echo scan generates two orders of magnitude more data than a transmission scan. The received echo provides data about each point along the path and not just the integral of attenuation over the path, as is the case with transmission tomography.

Basic approaches

Three basic approaches are investigated for estimating attenuation and backscatter: error correction, direct computation, and image iteration. The error correction approach is similar to the method proposed by Duck and Hill [1]. Initially, the attenuation and backscatter are set to nominal, uniform values. These images are corrected iteratively by using echoes from successive transducer positions. Each echo sample value is processed, starting with the nearest. The echo value E_R at each range R is compared to an echo value computed from the current estimates of attenuation and backscatter \hat{E}_R , where

$$\hat{E}_R = E_o \, \sigma_R R^{-2} \exp\left(-2 \sum_{j=1}^R \alpha_j \Delta S_j\right),\tag{1}$$

with σ_R as the current estimate of backscatter and α_j the current estimates of attenuation values along the echo path to range R, and with ΔS_j as the distance between echo samples. (In this discussion, the echoes are assumed to be normalized; i.e., $E_o=1$). The error between E_R and \hat{E}_R is used to correct the values of backscatter and attenuation in the image elements along the echo path. Several methods of correction were tried, including the use of different weights between the corrections to attenuation and backscatter, the use of damping factors, and the use of repeated imaging. In our studies all methods were unsatisfactory. The basic approach of error correction can produce images with large artifacts or that sometimes will not converge to an image.

The direct computation approach does not require an initial image which is iteratively refined. In this method two perpendicular linear scans are used to obtain as many echo values as unknown values of attenuation and backscatter. Figure 1 illustrates this approach. There are N scan positions

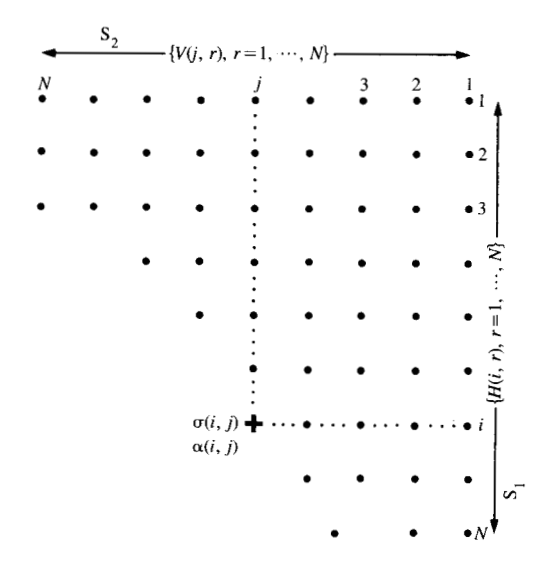


Figure 1 Geometry of direct computation.

and N range samples. The range sampling is selected so that the echo measurement points coincide. In this illustration, there are $2N^2$ unknowns and echo values.

The images of attenuation and backscatter are computed directly by inverting certain linear equations. Since the dimension of the linear equation set is large, it is convenient to solve it iteratively. Let H(i, k) be the echo values from the horizontal scans S_1 and V(i, k) be the echo values from the vertical scans S_2 (see Fig. 1). The attenuation and backscatter values are $\alpha(i, k)$ and $\sigma(i, k)$, with $\alpha(1, 1)$ and $\sigma(1, 1)$ corresponding to the upper right corner. Assume that the first k rows and columns of α and σ are estimated. Then the (k + 1)th row and column are given by

$$\sigma(i, k+1) = H(i, k+1)R_{k+1}^{2} \exp\left(2\sum_{j=1}^{k} \alpha(i, j)\Delta S\right),$$

$$\sigma(k+1, i) = V(i, k+1)R_{k+1}^{2} \exp\left(2\sum_{j=1}^{k} \alpha(j, i)\Delta S\right),$$

$$\alpha(i, k+1) = 0.5 \ln\left[\frac{\sigma(i, k+1)}{R_{i}^{2}V(k+1, i)} \frac{R_{i-1}^{2}V(k+1, i-1)}{\sigma(i-1, k+1)}\right],$$

$$\alpha(k+1, i) = 0.5 \ln\left[\frac{\sigma(k+1, i)}{R_{i}^{2}H(k+1, i)} \frac{R_{i-1}^{2}H(k+1, i-1)}{\sigma(k+1, i-1)}\right],$$

for $i=k+1, \cdots, N$. Even though this is a direct computation without constraints or arbitrary correction criteria (as used in the error correction approach), this approach is also unstable. Small perturbations in one parameter (attenuation or backscatter) can couple into the other parameter in a way that causes divergence. Even with

747

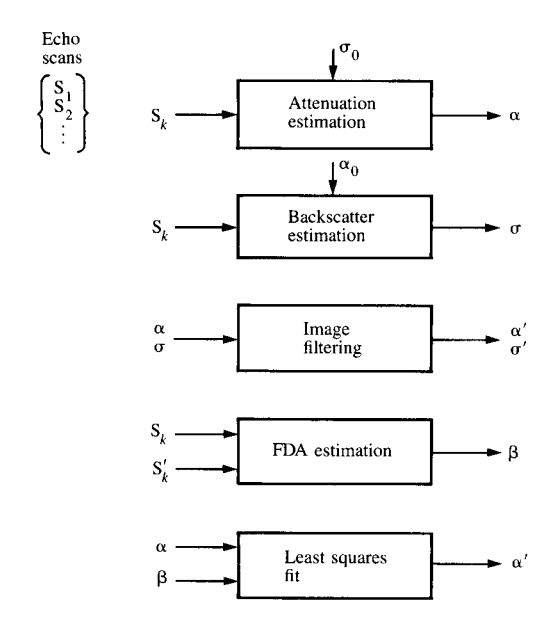


Figure 2 Image iteration functions.

damping factors and filtering in the estimation sequence, the method can diverge with simple or even uniform target fields.

Image iteration is the third approach. It differs from the error correction and direct estimation approaches in that the coupling between attenuation and backscatter does not occur locally along an echo path. Instead, the attenuation image is estimated using a uniform, fixed backscatter image; then the backscatter image is estimated using the computed attenuation image, for example. Cross-coupling between the attenuation and backscatter estimates is minimized with multiple scan directions, image filtering, and suitable image iteration. This image iteration approach is stable and is the approach developed in this study.

Estimation is based on Eq. (1). With a specified image of attenuation (or backscatter) and the echo measurements, backscatter (or attenuation) is estimated. Conceptually, images can be computed with a single scan, such as S₁ or S₂ in Fig. 1. The overall approach of image iteration is to strive for an optimal sequence of image scanning, filtering, and estimation of attenuation and backscatter. The basic functions are illustrated in Fig. 2. For example, scans S₁ and S₂ are used to estimate attenuation with a uniform backscatter image. This image is filtered and used to estimate backscatter, again using S₁ and S₂. Certain artifacts in these images of attenuation and backscatter are reduced by repeating the estimation sequence using a third scan with the current images as the starting values. The final images are found to be insensitive to the value selected for the initial uniform image.

Two other functions are included in Fig. 2. If echo data are available at two frequencies, an image of the frequency dependence of attenuation β is also estimated, i.e., the slope of attenuation vs frequency. The last function in Fig. 2 is a least squares fit of the estimated frequency-dependent attenuation (FDA) image to the estimated attenuation image; a scale factor and zero level are selected for the estimated FDA image to minimize its rms deviation from the estimated attenuation image. This yields a new estimate of attenuation. It is based on the assumption that changes in β and α are correlated; i.e., the spatial distribution of changes in β is the same as that in α . The magnitude of α is estimated by the least squares fit of scale factor and zero level. A major objective of this research is to determine the best sequencing of these five functions and scan directions to minimize image estimation errors.

• Estimation model

The estimation of attenuation, backscatter, and frequency-dependent attenuation in Fig. 2 is approached from a modeling viewpoint. A mathematical model is selected for the interaction between the ultrasound pulse and the tissue, for the scan mode, and for the space/time sampling. In this model, attenuation and backscatter are unknown two-dimensional arrays of parameters. The goal is to compute values for these arrays so that echoes simulated by the model are the same as the measured echoes (see Fig. 3). The arrays (or images) are a more physically relevant interpretation of the echo data, and are not an exact measurement of attenuation and backscatter.

For the estimation model, several assumptions are made. The transmitted beam is not refracted and does not have width. The backscatter is isotopic and frequency-independent (or known and corrected when estimating β). An image field is selected which covers the region of interest. The field is divided into squares; backscatter, attenuation, and frequency-dependent attenuation are constant in each square. (In this study, the image field is 50×50 mm and each square is 1×1 mm.) A simple case is shown at the bottom of Fig. 3 to explain the model. Points P_1, P_2, \cdots are the locations of echo samples $E_1, E_2 \cdot \cdot \cdot$; points $C_1, C_2, \cdot \cdot \cdot$ are the locations where the beam path crosses the image grid lines. Segments (C_1, P_2) , (P_2, C_2) , (C_2, C_3) , \cdots have lengths L_1 , L_2 , L_3 , \cdots . Between the transducer and C_1 , attenuation and scatter are assumed to be zero; i.e., the transducer is outside of the image field and the target is inside of it.

The backscatter image $\sigma(i, j)$ is estimated based on the echo values and an initial attenuation image $\alpha_0(i, j)$ using Eq. (1). For example,

$$\sigma(3, 2) = E_3 R_3^2 \exp \left[2(L_1 \alpha_0(2, 3) + L_2 \alpha_0(2, 3) + L_3 \alpha_0(3, 3) + L_4 \alpha_0(3, 2)) \right],$$

where R_3 is the distance from the transducer to point P_3 . Several echo points may be in the same square from different transducer positions. The corresponding backscatter estimates are averaged. The estimation program also has the option of averaging these estimates with an existing estimate of backscatter.

The attenuation image $\alpha(i, j)$ is estimated based on the echo values and the estimated backscatter image $\sigma_0(i, j)$ using Eq. (1). The method is sequential outward on the ray. Each echo value yields an estimate of the integral of attenuation up to the echo point. The difference between successive integral values gives the average attenuation between echo points. For example,

$$0.5 \ln \left(\frac{\sigma(3, 2)}{R_3^2 E_3} \right) - 0.5 \ln \left(\frac{\sigma(2, 3)}{R_2^2 E_2} \right)$$
 (2)

is the integral of attenuation between P_2 and P_3 . This integral divided by $L_2 + L_3 + L_4$ is the average attenuation, say α' . Similarly, the echo values E_3 and E_4 give an average attenuation between P_3 and P_4 , say α'' . The estimate of $\alpha(3, 2)$ is then

$$(L_{\Delta}\alpha' + L_{5}\alpha'')/(L_{\Delta} + L_{5}).$$

Since there are no echo points between C_2 and C_3 , $\alpha(3, 3)$ is α' . From multiple scan directions, several estimates of attenuation may be obtained for each image cell. These values are averaged.

The method of estimating frequency-dependent attenuation is very similar to that for attenuation. Let \tilde{E}_j be the echo values at the higher frequency. Then

$$0.5 \ln \left(E_i / \tilde{E}_i \right) \tag{3}$$

is the integral of β up to P_j times the frequency difference. The difference between successive integrals yields an average value of β along the path and an image $\beta(i, j)$ using the method described above. In this model, it is implicitly assumed that the beam cross-section and path are the same for each frequency. The errors introduced by this assumption require additional research and are not considered here.

These estimation equations have been implemented in an APL program which permits the user to interactively select the sequence of estimation and filtering. After each estimation step, the images are displayed to select the next function. Typically, the total CPU time for the sequential estimation of backscatter and attenuation is less than one minute on an IBM 370/168 computer.

Data generation

Echo data are numerically generated to test the proposed estimation method of image iteration in Fig. 2. The model used to generate the echo data differs from the estimation

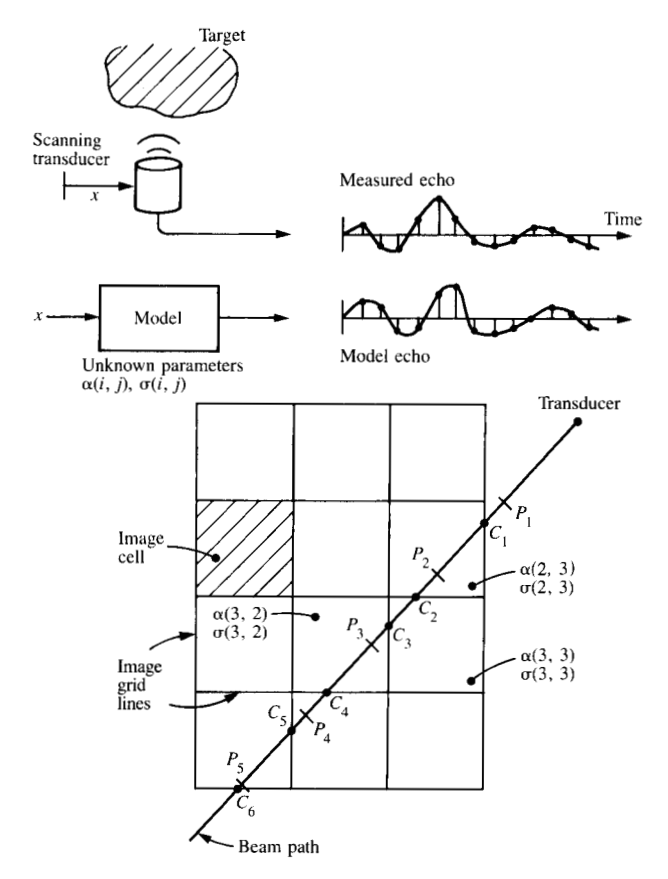


Figure 3 Geometry of estimation model.

model in several important ways. The target fields of attenuation and backscatter are continuous functions of position and are not segmented as in Fig. 3. The echo data are a result of a beam interacting with the target. The beam is formed from several rays spaced 0.8 mm apart at the transducer. Ray echo values from the same range are summed to form the echo beam values. The echo from each ray is

$$\frac{\sigma(x,y)+s(x,y)}{R^2}\exp\left(-2\int_0^R\alpha(x,y)\ ds\right),\,$$

where s(x, y) is image speckle. The speckle values at the echo points are modeled as uniformly distributed, independent random variables. Speckle represents anisotropic scatter from small scatter centers over the entire image. The effect on image quality depends on beamwidth, scan mode/direction, and the parameter that is imaged [6-10].

The beam is moved linearly in 0.8-mm increments over a distance of 72 mm, *i.e.*, 90 positions. Multiple linear scans are formed by rotating the scan line about the center of the image at a range of 36 mm. See Fig. 4. The value of this

749

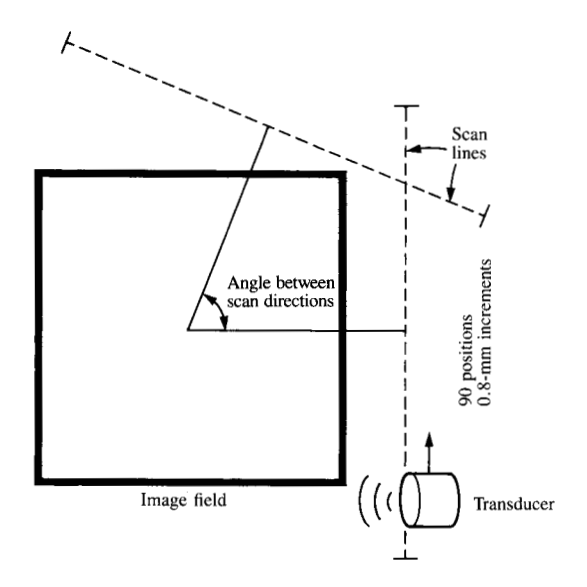


Figure 4 Scan geometry.

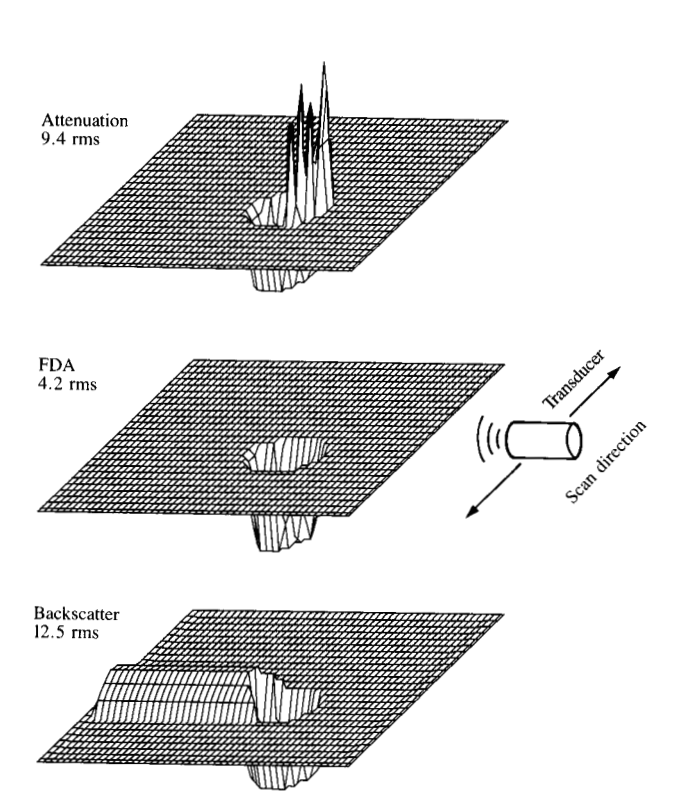


Figure 5 Estimated attenuation, frequency-dependent attenuation, and backscatter of a model cyst.

overall scan sector angle is between 60° and 150°, and in most cases is 90°. The return echo is sampled every 0.5 μs with 100 values used over the target.

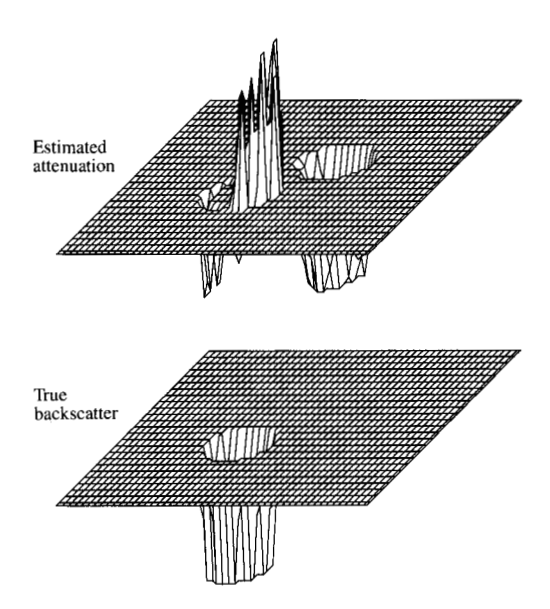


Figure 6 Error in estimated attenuation from assuming uniform backscatter.

The target is 50×50 mm and is composed of one or more objects (with circular or elliptical cross-sections) in a uniform background field of α , σ , and β . The values of α , σ , and β in the objects may be larger or smaller than the background. Typical biologic values were used [11–13]. The velocity is assumed to be uniform.

A single, cyst-like object was used in many of the studies. It is circular with a diameter of 10 mm and $\sigma=0.001$ mm², $\alpha=0.002$ nepers/mm, $\beta=0.001$ nepers/mmMHz. The background is uniform with $\sigma=0.01$ mm², $\alpha=0.02$ nepers/mm, and $\beta=0.01$ nepers/mmMHz. This object is used since it is of practical interest and it is a difficult object to image with echo tomography. The cyst-like object results in strong cross-coupling between α and σ with large image artifacts.

Single scan imaging

To optimize the image iteration (i.e., the sequence of functions and scans illustrated in Fig. 2), the first step is to determine the basic characteristics of each estimation function. Attenuation, backscatter, and frequency-dependent attenuation are estimated without multiple scans, filtering, or iteration. The effects of beamwidth, backscatter speckle, and cross-coupling of attenuation with backscatter were investigated. A single cyst-like object was used.

The estimated values of α , σ , and β are shown in Fig. 5 in the absence of speckle and scan beamwidth (*i.e.*, a one-ray beam). The rms errors are the rms difference between the

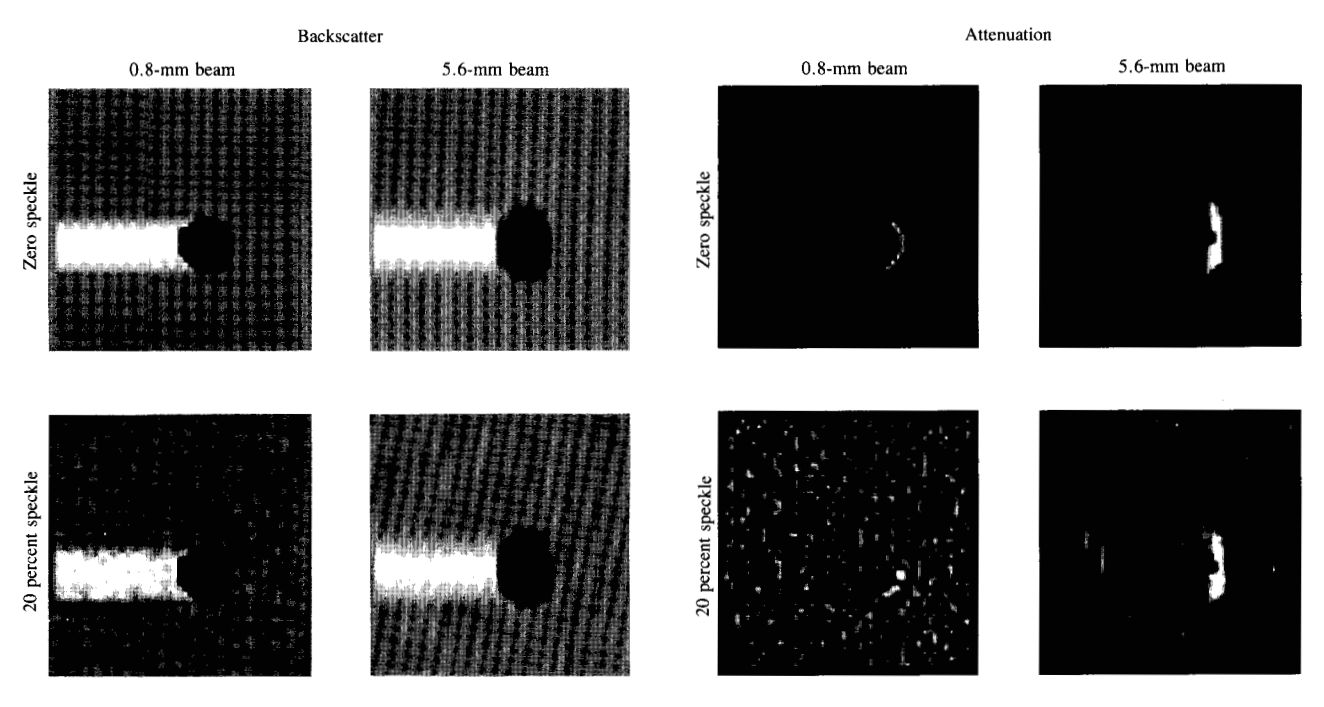


Figure 7 Estimated backscatter with a single linear scan.

Figure 8 Estimated attenuation with a single linear scan.

estimated and true values divided by the magnitude of the cyst object relative to background (expressed as percent). The initial values of attenuation and backscatter for estimation are uniform. In the case of frequency-dependent attenuation, the error of 4.2 is the residual error from image quantization. The backscatter is overestimated behind the cyst from the neglected low attenuation in the cyst region. The spikes in the attenuation image are the result of the neglected low backscatter in the cyst region. This is confirmed by moving the backscatter of the object relative to attenuation, as shown in Fig. 6. The spikes are only one image element wide and can be reduced with filtering. There is a fundamental difference between the cross-coupling of attenuation to backscatter and of backscatter to attenuation. An error in attenuation is integrated when estimating the backscatter image (bar behind cyst). An error in backscatter is differentiated when estimating the attenuation image (spikes). These error differences occur because attenuation appears in an integral in the estimation model, Eq. (1). Also, these errors depend on the scan direction, and can be reduced with multiple scan averaging.

The effect of 20 percent backscatter speckle and 5.6-mm beamwidth on backscatter imaging is shown in Fig. 7 (In some cases, there are edge artifacts that dominate the error computation. The artifacts are the result of the way data are generated; they are not relevant to this study. To avoid these edge artifacts, the edges of the images are set to the

background levels.) The effect of beamwidth is to spread the image in the scan direction, *i.e.*, cross beam. Also, the beam smooths the backscatter speckle; there tend to be random lines in the scan direction. Note that the imaging program scales the value between black and white.

The estimated attenuation images are shown in Fig. 8. With 20 percent scatter speckle, no satisfactory image of the cyst was obtained. With a 5.6-mm beam, the dark and light vertical bars are errors cross-coupled from the low backscatter in the cyst region. (If backscatter is uniform, the image is only rounded in the scan direction.) Also, note that the vertical size of the cyst image is about 4.5 mm. The basic reason for these artifacts is that the logarithms of the echo values are differenced to estimate attenuation, Eq. (2).

The images of frequency-dependent attenuation are shown in Fig. 9. Without a finite beamwidth, scatter speckle does not appear in the image. The backscatter is assumed to be frequency-independent (or corrected for frequency dependence); the magnitude of backscatter cancels in the estimation of frequency-dependent attenuation, Eq. (3). With a finite beamwidth, an artifact is obtained on the side farthest from the transducer. This is a result of the low backscatter in the cyst region. (If the backscatter is uniform, the image is only rounded in the scan direction.) Note that speckle noise occurs in the beam case only behind the cyst. These artifacts are different from those for attenuation since frequency-

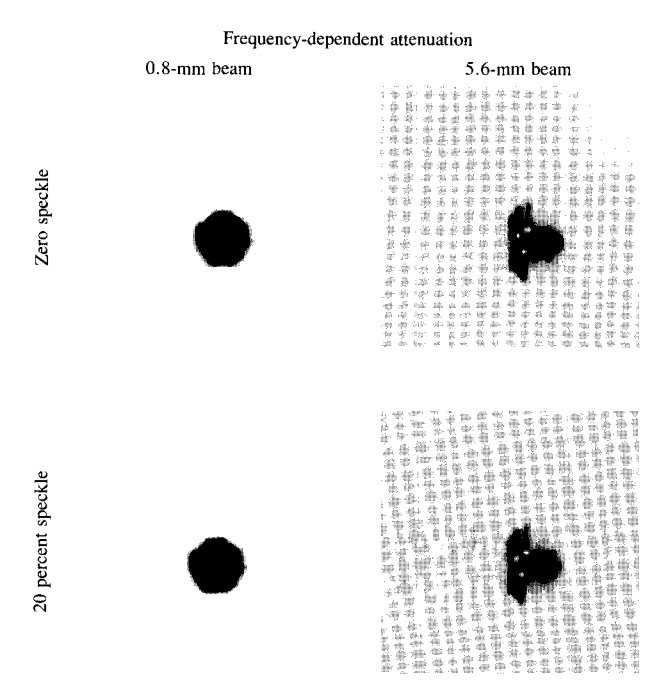


Figure 9 Estimated frequency-dependent attenuation with a single linear scan.

dependent attenuation is based on an echo ratio. The character of the image artifacts in Figs. 8 and 9 are predicted from a detailed mathematical analysis; the analysis is not presented because of its length and detailed nature.

The image artifacts illustrated in Figs. 7 through 9 are the result of beamwidth, backscatter speckle, and parameter cross-coupling. They can be minimized by optimally sequencing multiple scan averaging, pre- and post-image filtering, and iteration of image estimation. These basic methods are evaluated in the following three sections, and are the basis of the image iteration approach.

Multiple scan imaging

The image artifacts from beamwidth and parameter cross-coupling are dependent on scan direction. Averaging two images based on different scan directions improves the image quality. Attenuation and frequency-dependent attenuation images are shown in Fig. 10 for a 5.6-mm beam without backscatter speckle. The image artifacts in Figs. 8 and 9 are significantly reduced. The attenuation image has smaller error with a large angle between scan directions. The frequency-dependent attenuation image at 90° is qualitatively poorer than at larger or smaller angles. This is a result of the particular artifact with a beam (see Fig. 9). The backscatter image does not change qualitatively with the angle between scans. The rms errors are plotted in Fig. 11. A

scan angle between 90° and 120° is preferable. For smaller angles, the artifacts in attenuation and frequency-dependent attenuation are significant. For larger angles, the medical applications are more limited with little improvement in accuracy. Also, in real applications, the scatter speckle is likely to be less correlated for larger angles; hence, image averaging results in a greater reduction in speckling.

Averaging three or more images based on several scan directions does not significantly improve the final image. For example, if scans were made at 0°, 60°, and 120°, the attenuation image would be similar to the image for 120° in Fig. 10 with a brighter spot at the upper right edge. The additional scan at 60° shifts the distribution of errors, but does not improve the overall image.

From an image reconstruction viewpoint, linear scans are preferable to sector scans. For the same total number of sample points over the image field, the sector scans undersampled at large ranges; *i.e.*, some image elements may not be estimated. If the total number of points is increased for the sector scan, computation time and data storage are increased. Further, beam refraction occurs at the water/tissue interface; blind spots occur beyond the critical angle. These blind spots tend to be smaller with linear scans since most tissue surfaces are convex.

Image filtering

Pre- and post-image filtering is a second basic method of reducing image artifacts from beamwidth, scatter speckle, and parameter cross-coupling.

Pre-image filtering is done transversely and longitudinally with respect to the transmitted beam. Transverse filtering is achieved by beam deconvolution, *i.e.*, changing the effective beamwidth. Longitudinal filtering is achieved by filtering the return echo. The filtering is applied to data from two linear scans taken at a right angle to each other. This double-scan imaging is an important first step in reducing image artifacts, as shown above. To compare various filtering methods, the target is a single cyst whose diameter is 10 mm.

Decreasing the effective beamwidth with beam deconvolution has two contravariant effects. First, the cyst image distortion decreases with a decrease in beamwidth. This is shown in Fig. 12 for the cases with zero speckle. The rms errors in the images of attenuation and frequency-dependent attenuation decrease with effective beamwidth. The rms error in the backscatter image is nearly constant; the cyst image distortion decreases, but the cross-coupling error increases. Second, with backscatter speckle the image speckle "noise" increases with a decrease in effective beamwidth. The wider beam tends to smooth the effect of speckle in the image. The *total* rms error in the attenuation image

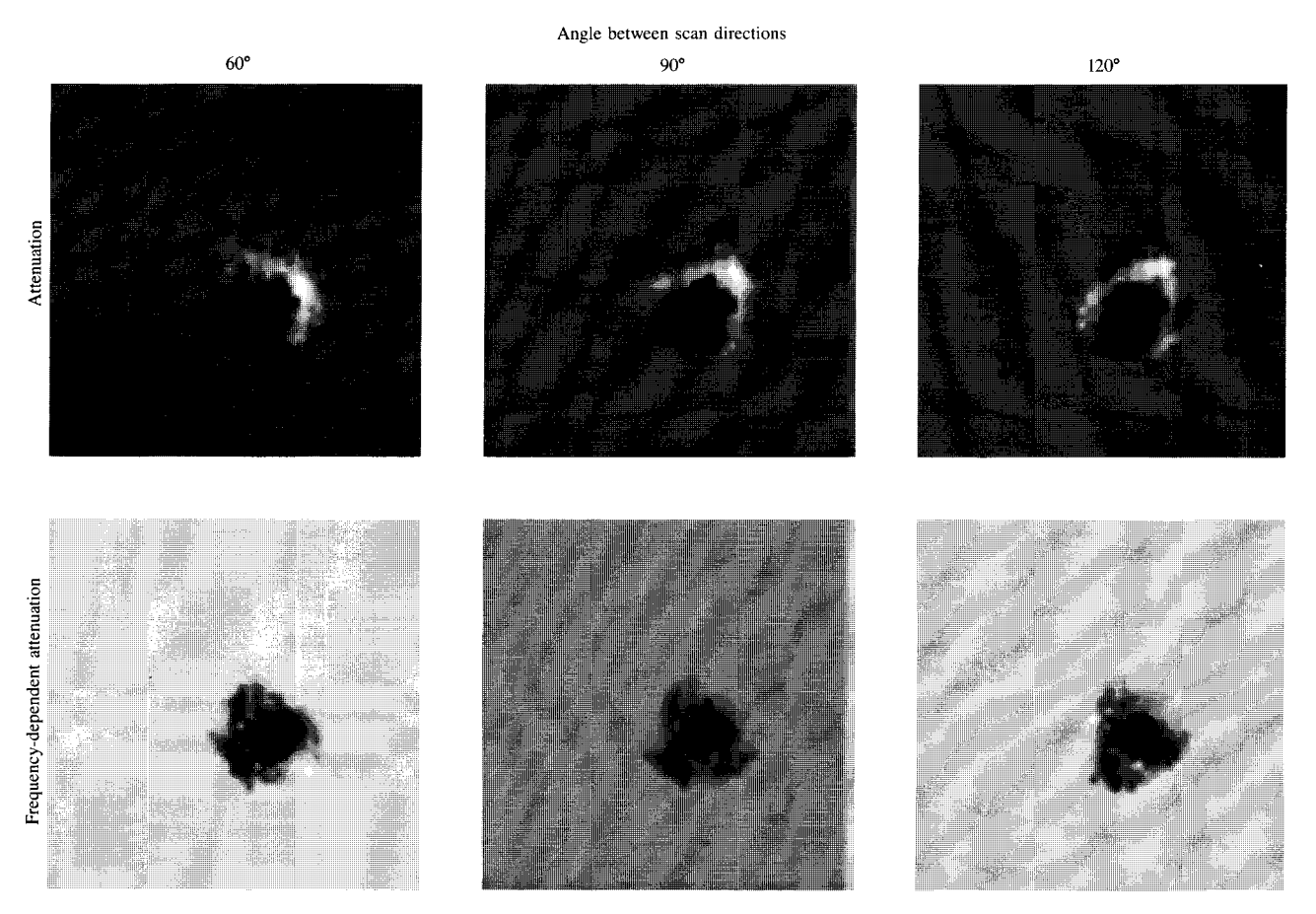


Figure 10 Attenuation and frequency-dependent attenuation with a 5.6-mm beam and zero speckle.

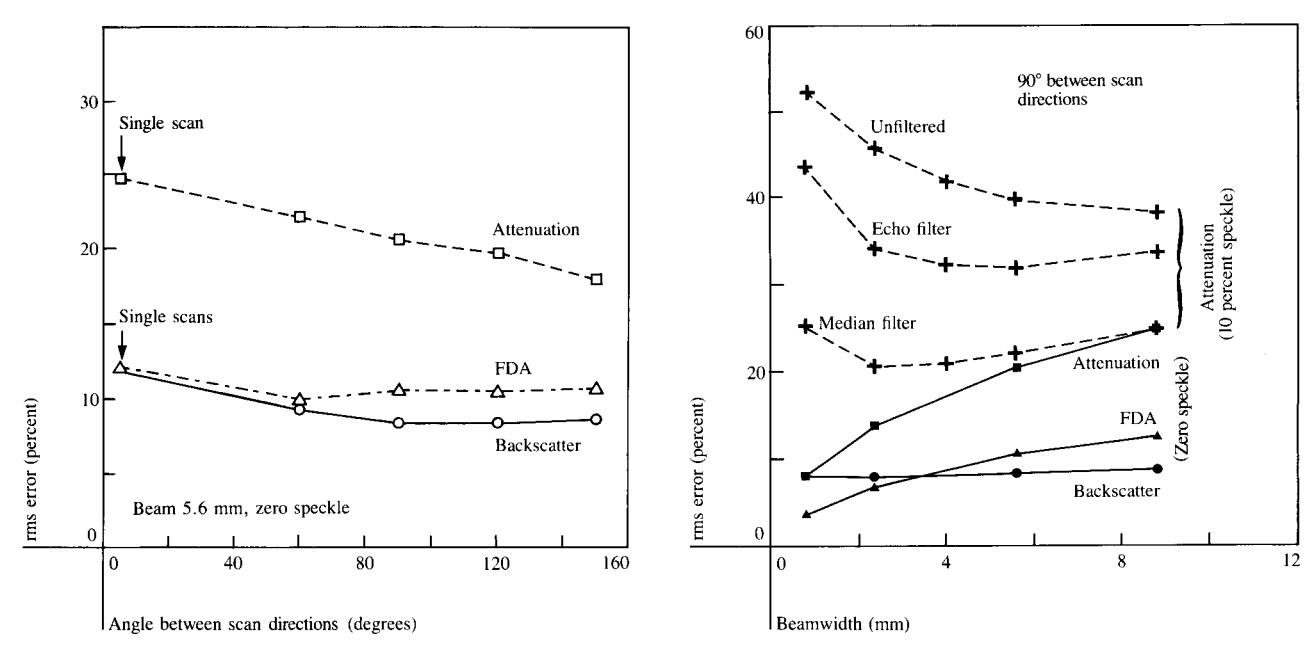


Figure 11 Error vs scan angle.

Figure 12 Error vs beamwidth.

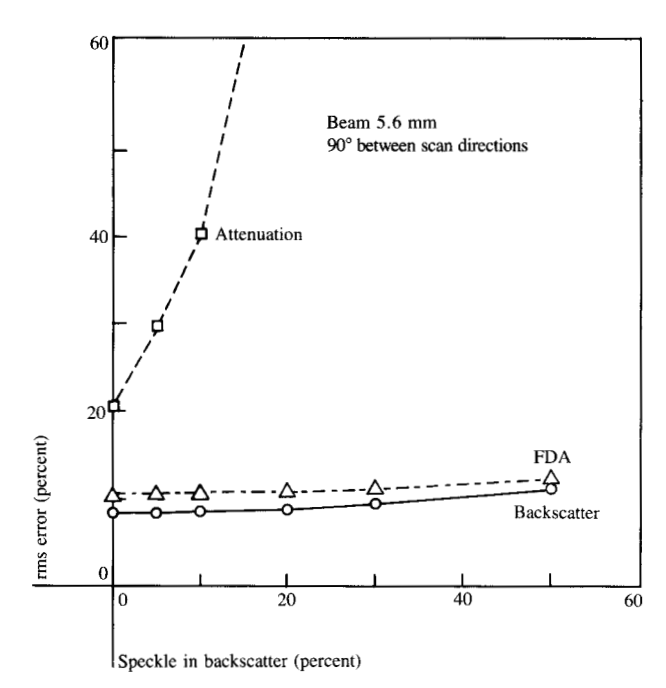


Figure 13 Error vs backscatter speckle.

increases with a decrease in beamwidth, even though the cyst image distortion decreases (Fig. 12, top curve). Image speckle noise is the dominant factor. Further, the total rms error in the attenuation image increases a large amount for a small increase in backscatter speckle (see Fig. 13).

Echo filtering decreases the large speckle error in the attenuation image. A case is shown in Fig. 12 where the echo is filtered with a sliding average over three values, which correspond to 2.25 mm in range. Even though the total error is decreased, the artifact of backscatter cross-coupling is increased, as shown in Fig. 14.

Several linear post-image filters are considered. The images are transformed to the Fourier domain, filtered, and inverse-transformed to form the filtered image. Low-pass filters [e.g., box-car, Gaussian, $(1 + \omega^2)^{-1}$] reduce the speckle effects and spikes from parameter cross-coupling; but they distort the cyst image. Since most of the unwanted artifacts are isolated transients, a median filter is very effective. Specifically, for each 3 × 3 matrix of image elements, the filter replaces the center value in the matrix by the median of the nine values. The median filter reduces the speckle noise and cross-coupling artifacts, as shown in Figs. 12 and 14. These results are based on two passes with the median filter. Additional passes did not improve the image significantly. Note that the median filter reduces the error in attenuation to the same level as zero speckle for beams greater than 4 mm.

Table 1 rms image error for different iteration sequences without backscatter. Speckle and beamwidth are 0.8 mm.

Iteration sequence	rms image error (%)		
	Backscatter	Attenuation	FDA
FDA		<u>-</u>	3.6
Backscatter	8.0	_	3.6
Attenuation	8.0	22.2	3.6
Filter	8.0	18.4	3.6
FDA	_	_	3.6
Attenuation		8.0	3.6
Filter		5.8	3.6
Backscatter	4.0	5.8	3.6
FDA —	****	_	3.6
Attenuation	_	8.0	3.6
Filter —	_	5.8	3.6
Attenuation -		4.0	3.6
Backscatter	4.0	4.0	3.6

Iteration

Iteration of image estimation and filtering is the third basic method of reducing artifacts from beamwidth, backscatter speckle, and parameter cross-coupling. The image iteration approach (Fig. 2) is based on using intermediate images in subsequent steps with filtering to obtain the final images of backscatter, attenuation, and frequency-dependent attenuation.

A basic iteration option is whether to estimate attenuation and then backscatter using the attenuation estimate or to estimate backscatter then attenuation using the backscatter estimate. To evaluate the implicit accuracy of these options, a simple cyst target was used without backscatter speckle or beamwidth. Two linear scans spaced 90° apart were used. The results are compared in Table 1. In the first sequence, the 3.6 percent error in frequency-dependent attenuation is a result of image quantization. The major cause of the 8.0 percent error in backscatter is cross-coupling from an initial uniform attenuation image, *i.e.*, bright bands behind the backscatter image like those in Fig. 7. These errors cause the large 22.2 percent errors in the attenuation image. Two passes with a median filter do not significantly reduce this error.

In the second sequence, the attenuation is estimated based on a uniform backscatter image. The 8.0 percent error results from cross-coupling, *i.e.*, a bright spot on the near side of the image (Fig. 10). Two passes with a median filter reduce the error to 5.8 percent. Using this attenuation image, the estimated backscatter image has 4.0 percent error, which is near the error obtained for frequency-dependent attenuation. If this sequence is extended by estimating attenuation using

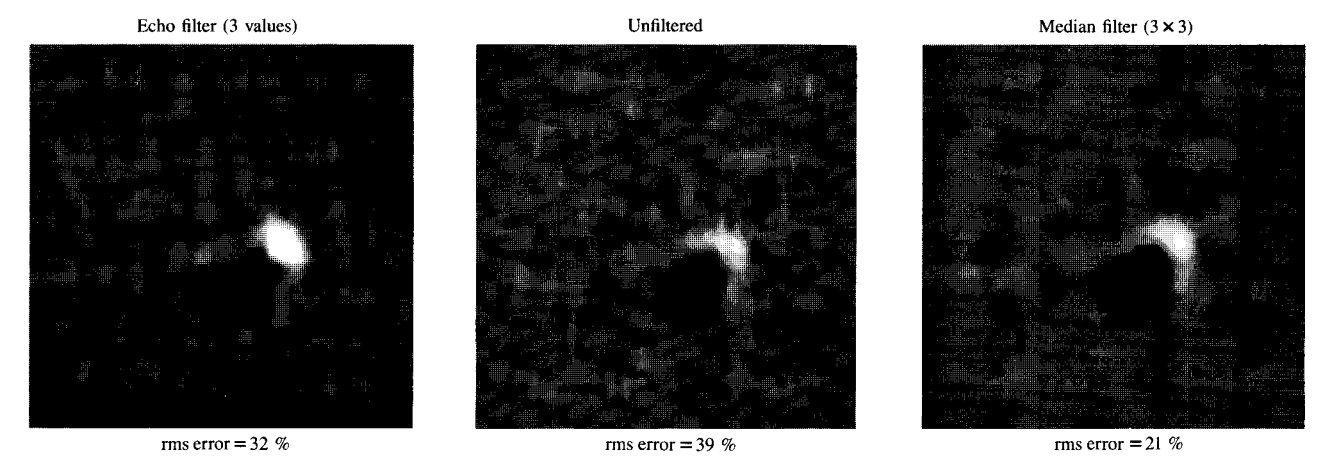


Figure 14 Attenuation image with 5.6-mm beam and 10 percent speckle.

the last backscatter estimate, the attenuation image has a very large error similar to the first sequence.

The third iteration sequence in Table 1 uses a least squares estimate of attenuation based on initial estimated frequency-dependent attenuation and attenuation. With this iteration sequence, a minimal error is achieved for all three estimates. Even though the third sequence is more accurate than the second, the second sequence is considered since it may not be feasible to estimate FDA with some ultrasound systems. Note that the direct estimates of attenuation and backscatter have errors of 22.2 and 8.0 percent, respectively.

To evaluate the effect of image iteration on shape-dependent errors, shadowing, and resolution, a complex target is used. It contains backscatter and attenuation objects with values both larger and smaller than the background levels, as shown in Fig. 15. The scanning beam is 4 mm wide, which is comparable to the 5-mm objects in the target. Two linear scans are made at right angles and parallel to the x and y axes.

From each linear scan, a backscatter image is obtained assuming that attenuation is uniform. Two composite images are formed by averaging the backscatter values and by taking the maximum backscatter value at each image element (Fig. 16). Both images are median filtered. The average image has a large error at location A since echoes received in the x scan from A are strongly attenuated by the target element. The maximum backscatter image is more accurate, but still there is a significant error at B. Also, the target element at C in both images is significantly diminished by shadowing from the highly attenuating elements closer to the transducer.

Image iteration significantly improves the backscatter image as shown in Fig. 16. Even though the estimated

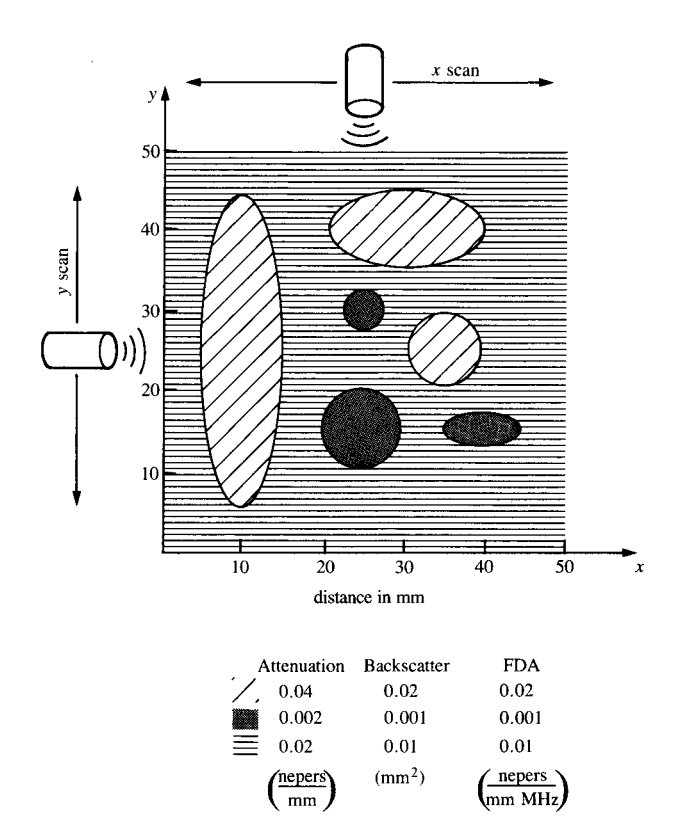


Figure 15 Complex target.

attenuation image has significant transients from crosscoupling, the backscatter estimate is within 9 percent of the true image. The error of the attenuation image is 17 percent. The beamwidth of 4 mm causes the reduced image sharpness. Both attenuation and backscatter have been median filtered. Using an estimate of frequency-dependent attenua-

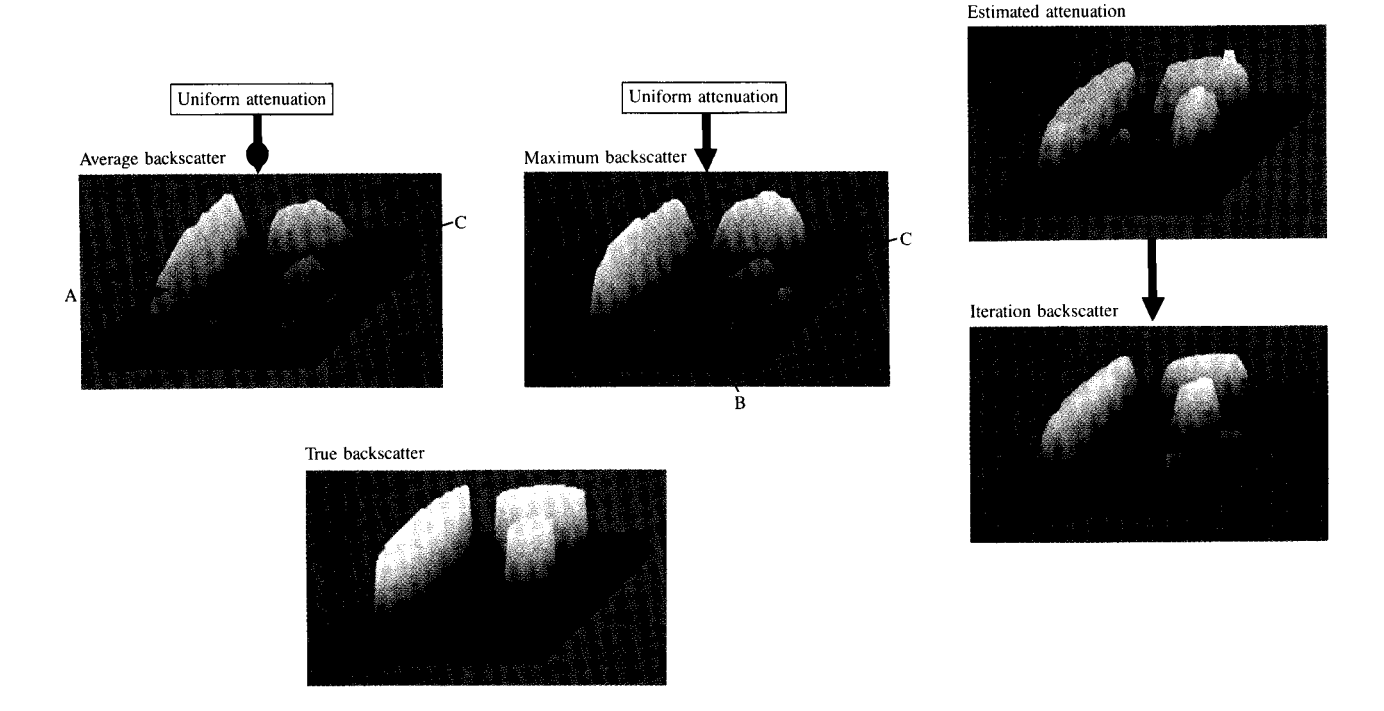


Figure 16 Backscatter estimation with and without iteration.

tion to improve the attenuation image (Table 1, third sequence), the errors in backscatter and attenuation are reduced to 7.3 and 10 percent, respectively.

With 10 percent backscatter speckle, it is necessary to use an estimate of frequency-dependent attenuation because a direct estimate of attenuation has large errors. The sequence of images is shown in Fig. 17. The target elements are poorly defined in the original attenuation image (32.6 percent error). Because of beamwidth, speckle is imaged as vertical and horizontal bars which correspond to the scan directions [6, 7]. After image iteration with FDA and median filtering, the elements are distinct with 14.7 percent error. The error in backscatter is 8.9 percent. An image based on maximum-backscatter estimation is presented for comparison. Note that there is a large distortion in the amplitude of the 10-mm object, A.

Discussion

From a mathematical viewpoint, estimation of backscatter and attenuation is feasible; *i.e.*, there are at least as many linearly independent equations as there are unknown values of backscatter and attenuation in the image field. From a practical viewpoint, there are many significant problems, *e.g.*, computational convergence and accuracy, optimal scan configuration, beam and estimation artifacts, backscatter speckle errors, and the effects of refraction, anisotropic

backscatter, and reflection. In estimating frequency-dependent attenuation, the effects of phase cancellation and the variation of beamwidth with frequency require particular consideration. Several of these errors are minimized in the development and evaluation of the image iteration approach.

Image iteration is a practical computational approach which converges to images which are typically within 10 percent of the true image. The effects of backscatter speckle, beamwidth artifacts, and parameter cross-coupling are minimized with multiple scans, image filtering, and iteration. Alternate approaches, based on error correction or direct computation, diverge in some cases or converge to images with large errors.

The estimates of backscatter and attenuation have two significant properties which facilitate error reduction. First, the error in attenuation cross-coupled from backscatter (Fig. 3) is one image element in size. It can be markedly reduced by median filtering. Second, beam artifacts and cross-coupling errors depend on the scan direction (Figs. 7, 8, and 9). Imaging, based on two scans 90° to 120° apart, cancels a major portion of these errors. In clinical applications, more than two scans may be helpful to reduce the effects of shadows, image dropout, anisotropic backscatter, reflecting layers, etc.

756

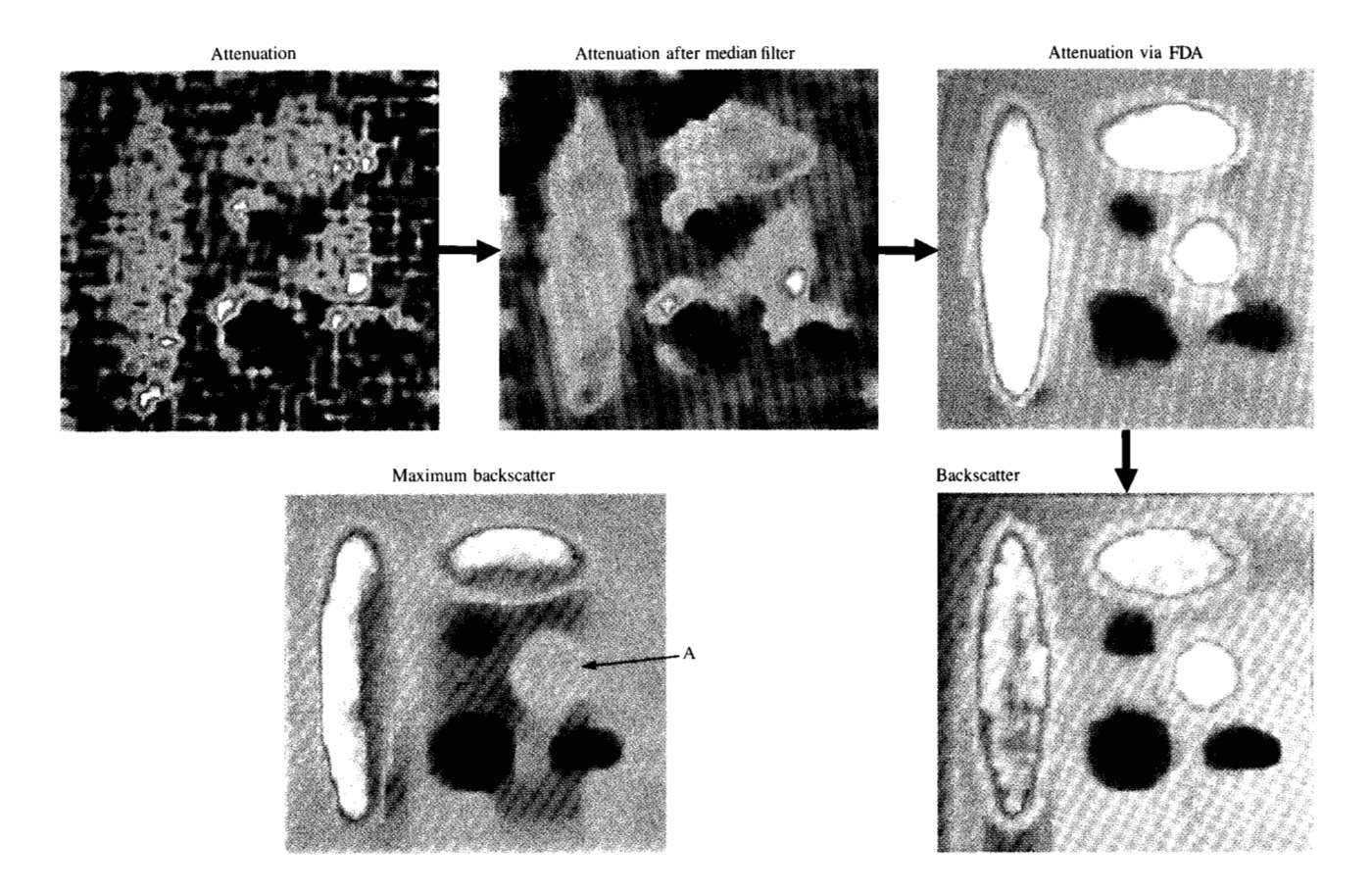


Figure 17 Image iteration of attenuation and backscatter with 10 percent speckle.

The errors in estimating backscatter neglecting the effect of attenuation are large, but they can be minimized with image iteration (Figs. 16 and 17). In clinical applications, the optimum sequence of imaging and filtering may vary depending on the region scanned, the structure of interest, transducer beam characteristics, and scan orientations.

The results of this study indicate that image iteration is a feasible approach to estimate attenuation, backscatter, and frequency-dependent attenuation. The final evaluation of image iteration requires a wide range of patient scans and calibrated studies of tissue phantoms. This evaluation is currently in progress. Preliminary results on images of backscatter and attenuation obtained from patient scans are qualitatively consistent with known ultrasonic properties of the tissues.

A key aspect of clinical imaging is to obtain scan data that are proportional to the magnitude of the received echo. The effects of logarithmic amplitude compression and Time Gain

Control must be minimized. The resulting images have a wide dynamic range. An interactive three-dimensional graphic package, IMAGE3D [14], has been developed which enables the user to display images which have a wide range of intensities. It includes five display modes and several editing features for detailed interpretation of the images. The images in this paper were formed with IMAGE3D. An interactive, flexible image reconstruction program and graphic display are essential to minimize errors and fully extract the information in backscatter and attenuation images. The image iteration approach described in this study and the graphics package IMAGE3D satisfy these needs.

Acknowledgment

This work was supported in part by National Science Foundation University/Industry Joint Research Grant ECS 80–17683 with the University of Rochester, New York. As principal investigators, Professor Robert Waag of the University of Rochester and C. N. Liu of IBM have given helpful suggestions during the course of this research study.

References

- F. A. Duck and C. R. Hill, "Acoustic Attenuation Reconstruction from Back-scattered Ultrasound," in Computer Aided Tomography and Ultrasonics in Medicine, J. Raviv, J. F. Greenleaf, and G. T. Herman, Eds., North-Holland Publishing Co., Amsterdam, 1979.
- R. W. Rowe, "Ultrasonic Image Reconstruction," Report UKSC 107, IBM UK Scientific Centre, Winchester, England, 1981.
- 3. G. Maderlechner, E. Marschall, and E. Hundt, "Improvement of Computerized Ultrasonic Echo Tomography by B-scan Techniques," 6th International Symposium on Ultrasonic Imaging and Tissue Characterization, National Bureau of Standards, Gaithersburg, MD, May 1981 (abstract).
- R. Kuc, "Clinical Application of an Ultrasound Attenuation Coefficient Estimation Technique for Liver Pathology Characterization," *IEEE Trans. Biomed.* 27, 312-319 (1980).
- A. Johnson, J. F. Greenleaf, M. Tanaka, R. Rajagopalan, and R. C. Bahan, "Reflection and Transmission Techniques for High Resolution, Quantitative Synthesis of Ultrasound Parameter Images," *IEEE Ultrasonics Symposium Proceedings*, 1977, pp. 983-988.
- S. W. Flax, G. H. Glover, and N. J. Pele, "Textural Variations in B-mode Ultrasonography: A Stochastic Model," *Ultrasonic Imaging* 3, 235-257 (1981).
- 7. P. N. T. Wells and M. Halliwell, "Speckle in Ultrasonic Imaging," *Ultrasonics* 19, 225-229 (1981).
- C. B. Burckhardt, "Speckle in Ultrasound B-Mode Scans," IEEE Trans. Sonics Ultrasonics SU-25, 1-6 (1978).
- J. G. Abbot and F. L. Thurstone, "Acoustic Speckle: Theory and Experimental Analysis," *Ultrasonic Imaging* 1, 303-324 (1979).
- L. J. Busse and J. G. Miller, "A Comparison of Finite Aperture Phase Sensitive and Phase Insensitive Detection in the Near Field of Inhomogeneous Material," *Proceedings of the 1981 IEEE Ultrasonics Symposium*, Catalog Number 81CH1689-9, 1981, pp. 617-626.
- P. Bhagat, M. Kadaba, R. Ware, and W. Cockerill, "Frequency Dependence of Acoustic Parameters of Freshly Excised Tissues of Sprague Dawley Rats," *Ultrasonics* 17, 179–182 (1977).

- R. C. Chivers and R. J. Parry, "Ultrasonic Velocity and Attenuation in Mammalian Tissues," J. Acoust. Soc. Amer. 63, 940-953 (1978).
- 13. M. O'Donnell, J. W. Mimbs, and J. G. Miller, "The Relationship between Collagen and Ultransonic Attenuation in Myocardial Tissue," J. Acoust. Soc. Amer. 65, 512-517 (1979).
- E. J. Farrell, "IMAGE3D(version 2): APL Graphics Package for 3D Imaging," Research Report RC 9303, IBM Thomas J. Watson Research Center, Yorktown Heights, NY, 1982.

Received March 17, 1982; revised May 26, 1982

Edward J. Farrell IBM Research Division, P.O. Box 218, Yorktown Heights, New York 10598. Mr. Farrell joined the Research Division as a research staff member in 1968. His current research is on image reconstruction and multidimensional color presentation of images and data. Prior studies involved the application of simulation and statistical methods to evaluate and predict the likely recovery of critically ill patients. From 1966 to 1968, he was principal mathematician at UNIVAC, St. Paul, Minnesota. Mr. Farrell's work involved processing techniques and simulation related to spacecraft stabilization. From 1964 to 1966, he was a senior research scientist in the Research Division of Control Data Corporation. His research was concerned with feasibility and accuracy of different scanning optical sensors for celestial navigation. From 1959 to 1964, he was a mathematician in the Mathematics and Logic Research Department of UNIVAC, St. Paul. His assignments involved development of signal processing techniques related to sonar target classification and computer system reliability. Mr. Farrell received a B.S. from the University of Minnesota with a major in physics, and subsequently completed his doctoral course work in mathematical statistics. In 1982, he received an IBM Outstanding Technical Achievement Award for his work related to patient recovery.